SUPPLEMENTARY DATA

Figure S1

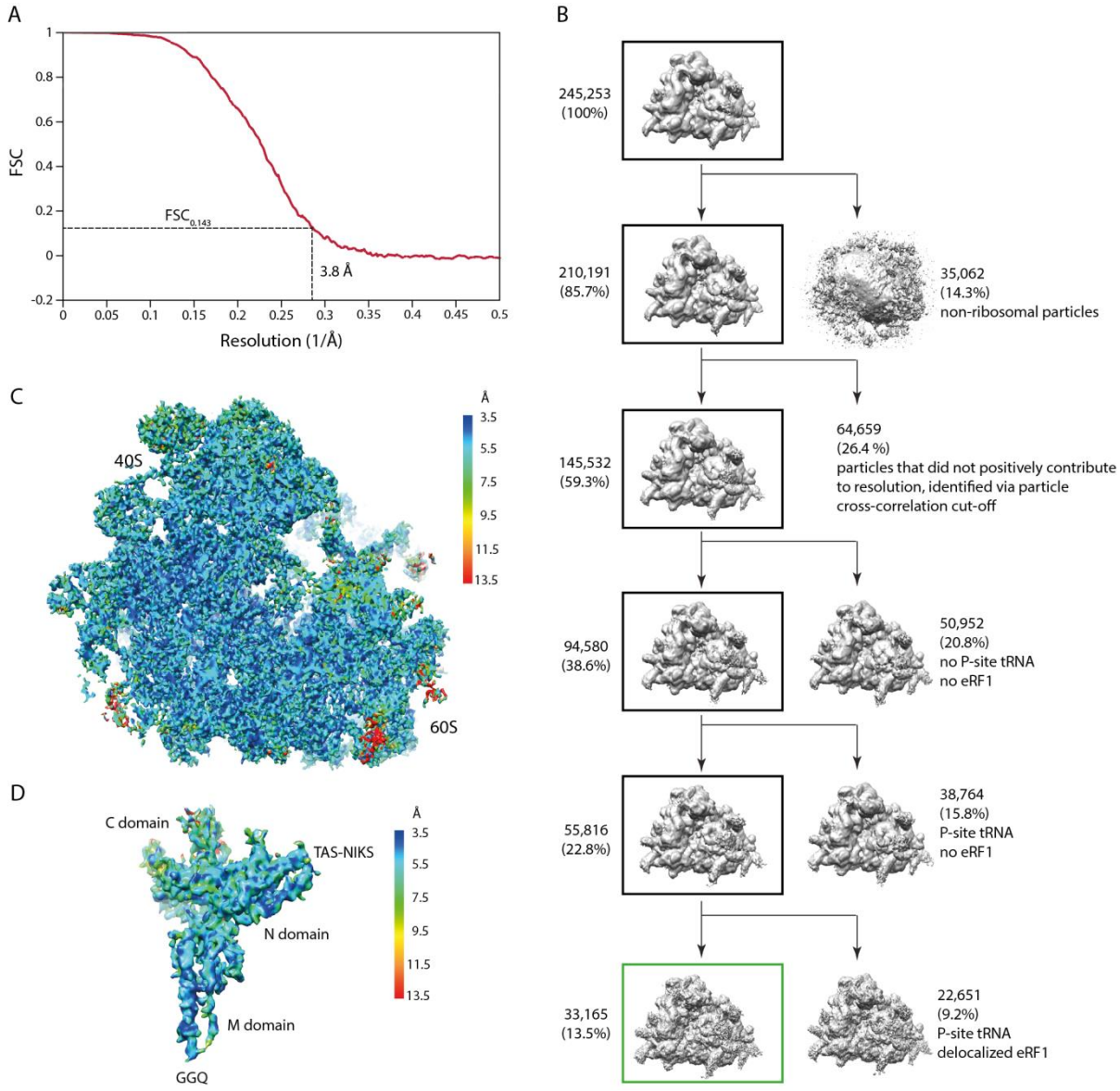

Figure S1 Average resolution, local resolution and particle sorting scheme of the cryo-EM reconstruction.

(A) The average resolution of the final reconstruction of the eRF1 bound 80S-CMV-RNC was estimated to be 3.8 Å based on the Fourier shell correlation (FSC) cut-off criterion at 0.143. The FSC was derived from half-map reconstructions processed in the absence of spatial frequencies higher than 8 Å (see also Material and Methods). **(B)** *In silico* particle sorting scheme for obtaining the final dataset. **(C)** Section of the cryo-EM map of the eRF1 bound 80S-CMV-RNC colored according to the local resolution as calculated by the ResMap software. **(D)** Local resolution of isolated eRF1 in the cryo-EM map colored as in (C).

Figure S2

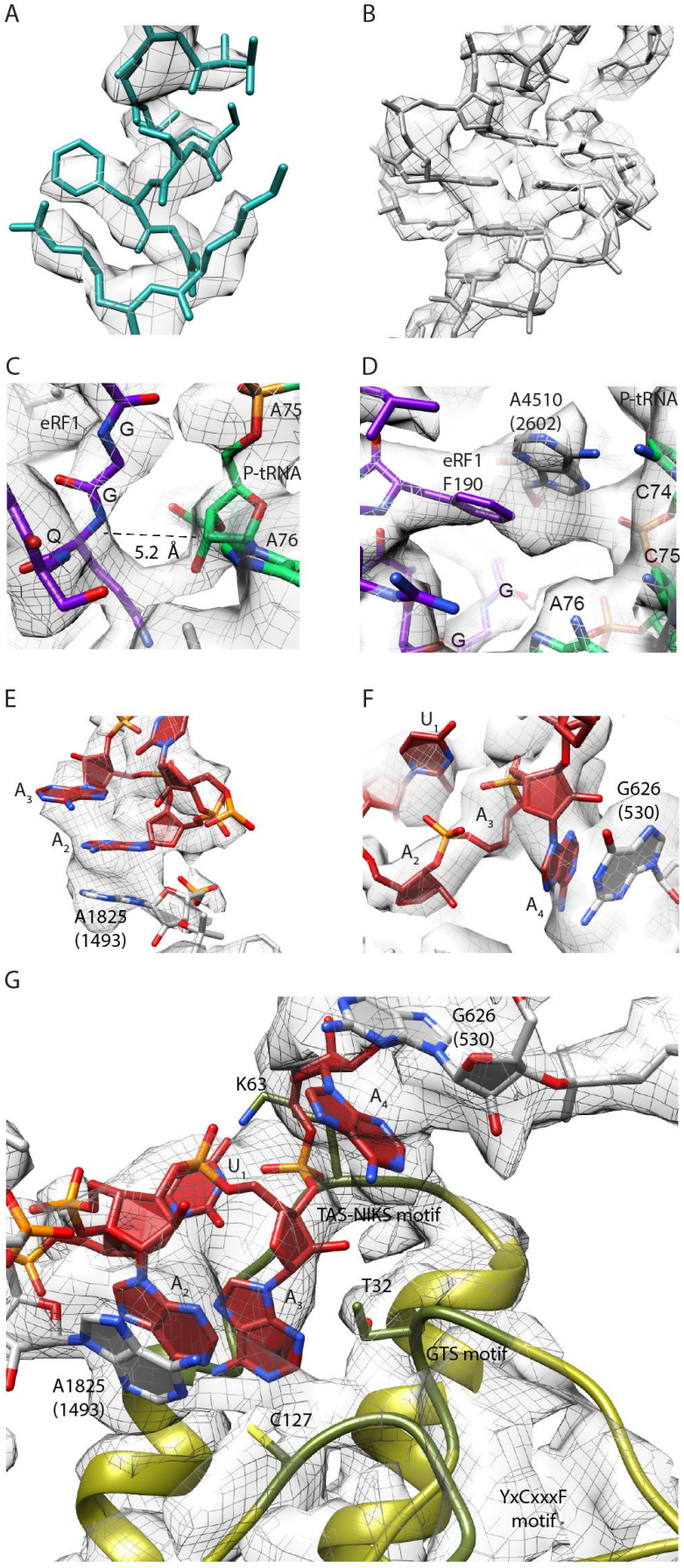
A
B
C
eRF1
G
G
Q
A75
P-tRNA
5.2 Å
A76
D
A4510
(2602)
P-tRNA
eRF1
F190
C74
C75
G
A76
G
E
A3
A2
A1825
(1493)
F
U1
A3
A2
A4
G626
(530)
G
G626
(530)
K63
A4
U1
TAS-NIKS motif
A2
A3
T32
GTS motif
A1825
(1493)
C127
YxCxxxF
motif

Figure S2 Electron density representation of selected regions.

(A, B) Electron density (gray mesh) for selected regions of the large ribosomal subunit; **(A)** ribosomal protein and **(B)** rRNA. **(C)** Electron density (gray mesh) for the human eRF1 GGQ-motif (purpleblue) and the peptidyl-tRNA nucleotides C75, A76 (green) within the PTC as shown in Figure 3E. **(D)** Electron density (gray mesh) for the interaction between the base *Hs* A4510 (*Ec* 2602) and eRF1 F190 (purpleblue) as shown in Figure 3G. The peptidyl-tRNA CCA end is shown in green. **(E)** Electron density (gray mesh) for the base stacking interaction of the UAA(A) stop codon (A_2, A_3) with rRNA base *Hs* A1825 (*Ec* 1493). **(F)** Electron density (gray mesh) for the stacking interaction of A_4 with rRNA base *Hs* G626 (*Ec* 530). **(G)** Electron density (gray mesh) for the interaction region of eRF1 with the stop codon UAA(A). The TAS-NIKS (residues 58-64), YxCxxxF (residues 125-131) and GTS (residues 31-33) motifs are colored in dark green.

Figure S3

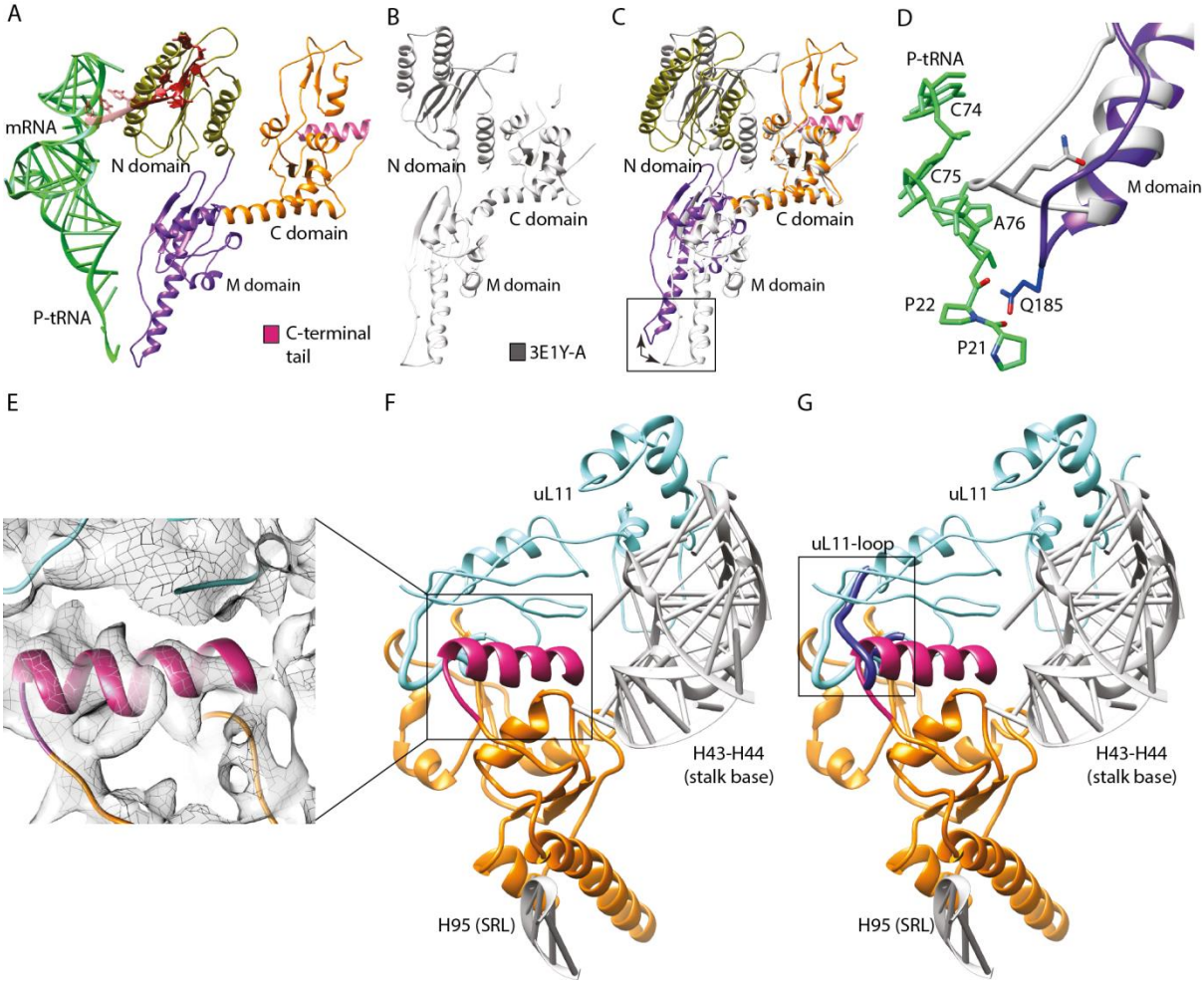

Figure S3 Comparison of ribosome-bound human eRF1 with the crystal structure.

(A) Ribosome-bound eRF1 in the context of mRNA and P-site tRNA color-coded as in Figure 2D except for the C-terminal tail of eRF1 (residues 421-437; pink). **(B)** Crystal structure of the human eRF1 (from the eRF1-eRF3 complex, Cheng *et al*. (12), pdb code: 3E1Y-A). **(C)** Overlay of the ribosome-bound eRF1 (colored) and eRF3-bound eRF1 (gray). Their alignment was based on the eRF1 C domain. **(D)** Alignment of ribosome-bound eRF1 (purpleblue) and eRF3-bound eRF1 (gray) based on the M domain with resulting overlay of close-up on the GGQ-motif. The GGQ-loop is remodeled in the ribosome-bound conformation positioning the conserved Q close to the ester bond between the terminal adenosine (A76) of the peptidyl-tRNA and P22 of the hCMV nascent peptide. **(E)** Close-up view of the filtered (approx. 4 Å) electron density of the C-terminal tail of eRF1 which forms an α-helical secondary structure and is not present in the crystal structure. **(F)** Molecular model for the eRF1 C domain bound to the stalk base of the LSU (uL11 and rRNA helices H43-H44). **(G)** The α-helix of the C-terminal tail of eRF1 (pink) accommodates into a pocket formed by the N-terminal domain of uL11. Thereby, it displaces the uL11-loop formed by residues 28-40 (dark blue loop), which moves towards the inter-subunit space (light blue loop) during eRF1 binding.

Figure S4

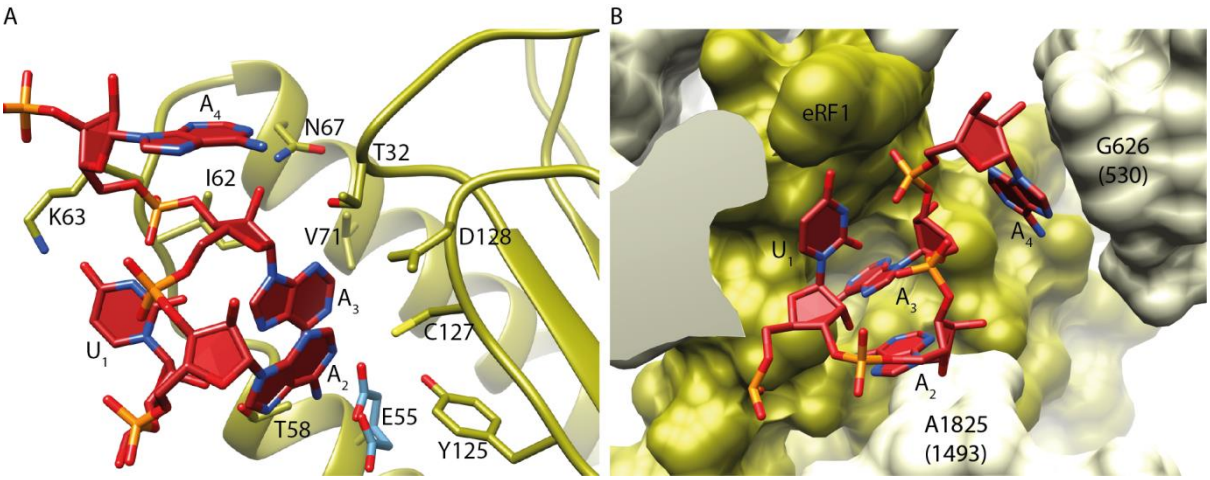

Figure S4 Binding pocket for the stop codon.

(A) Close-up view on the decoding cavity of the eRF1 N domain (olive) bound to the UAA(A) stop codon (dark red). Relevant residues described previously are depicted as atoms with heteroatoms. **(B)** Surface representation of the UAA(A)-binding cavity formed by the eRF1 N domain and rRNA in the decoding center of the small ribosomal subunit.